THE JOURNAL OF PHYSICAL CHEMISTRY C

Article

pubs.acs.org/JPCC

Spatially Sequential Growth of Various WSi_2 Networked Nanostructures and Mechanisms

Mohammad Norouzi Banis,[†] Xiangbo Meng,[†] Yong Zhang,[†] Mei Cai,[‡] Ruying Li,[†] and Xueliang Sun*[,†]

[†]Department of Mechanical and Materials Engineering, The University of Western Ontario, London, Ontario N6A 5B9, Canada

[‡]General Motors R&D Center, Warren, Michigan 48090-9055, United States

Supporting Information

ABSTRACT: Various WSi_2 nanostructures including networked nanorods (NNWs), networked nanoribbons (NNRs), and nanosheets (NSs) were sequentially (spatial) synthesized in a controlled manner via a single-step chemical vapor deposition method. Their morphology, structure, and composition were characterized by scanning and transmission electron microscopes and X-ray diffraction. The nanostructures are 6−10 nm in thickness and several micrometers in length. The results reveal that the formation of WSi_2 nanostructures is governed by a vapor solid mechanism and the concentration of reactive species plays a crucial role in controlling the formation of the various morphologies of the synthesized nanostructures. The time-dependent growth study shows that the nanostructures feature two-dimensional growth of WSi_2, resulting in nanonets and nanosheets. Cyclic voltammetry measurements of these nanostructures demonstrate the chemical capacitance characteristics of WSi_2 nanosheets and nanoribbons. Not only has this study paved a new route for preparing various nanostructures, but also these nanostructures are of great interest for nanodevices and electrochemical applications.

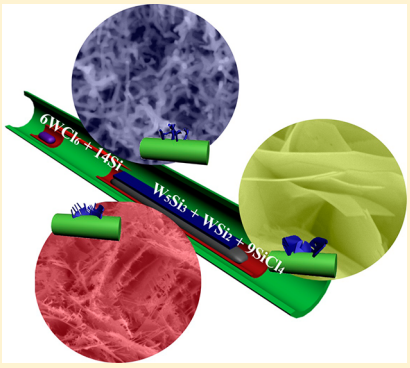

INTRODUCTION

The continuing dimensional shrinkage of conventional electronic devices requires new building blocks that are able to provide a higher device density, especially through their novel nanostructures.[1,2] Among potential materials, metal silicides, a family of refractory, intermetallic compounds between metals and silicon, have attracted much interest, especially in the field of electronics[3−8] and energy.[9−12] Research on these materials is driven by their distinguished properties, such as high electrical conductivity[1,3,4,13] and superior thermal[14] and chemical stability.[14−16] Metallic silicides including $TiSi_2$,[3,11] MnSi,[17] and NiSi[6,7,18] have been used as interconnects in electronic devices due to their low contact resistance. In addition, these materials are potential candidates for high-temperature applications as they usually have high melting points and show good oxidation resistance.[14,15,19,20]

Recent studies focused on synthesizing nanostructured metal silicides, such as Ti_5Si_3,[1] $TiSi_2$,[11] FeSi,[21] $NiSi_2$,[12] $CrSi_2$,[22] Fe_5Si_3,[23] Mn_5Si_3,[24] and $TaSi_2$,[25] have brought about some new physical phenomena and interesting applications.[3,6,11,26] However, synthesis of such materials with high melting points is still challenging. Previous studies demonstrated that complex nanostructures including nanonets or branched structures are favored to simple 1D nanostructures in many applications.[3,9,10,27,28] Consequently, they add additional challenges to the synthesis process. To overcome this difficulty, various efforts have been reported, for example, using silicon or metal nanowires as templates or chemical vapor deposition (CVD) methods via low-temperature precursors.[6]

Tungsten silicides (WSi_2, W_5Si_3) are among the refractory transition metal silicides and have a high oxidation resistance.[14,20,29] Further, researchers have reported that tungsten silicides exhibit superconducting properties and have been studied as prime candidates for replacing doped polysilicon of low resistivity.[13,30] To date, there have been no reports on growth of tungsten silicide nanostructures.

In this work, for the first time, we developed a facile method to synthesize high melting point tungsten silicide nanostructures from networked nanorods to nanoribbon to nanosheets by low pressure chemical vapor deposition (LPCVD). The method features the simultaneous growth of these nanostructures in different spatial zones. Through investigating time-dependent growth characteristics of these nanostructures, a growth mechanism was proposed.

EXPERIMENTAL METHOD

WSi_2 nanostructures were synthesized via a home-built LPCVD system. WCl_6 (Aldrich, 99.9%) and Si (Aldrich, 99%) powder were used as the starting materials. Carbon paper was used as the substrate. Carbon paper was chosen as the substrate due to their conductivity and porous structure, making them suitable for electrodes, for instance, as fuel cell backing in low-temperature fuel cells. The substrates were put on an alumina boat containing silicon powders. The source materials and

Received: May 5, 2013
Revised: August 6, 2013
Published: August 13, 2013

   dx.doi.org/10.1021/jp404444p | J. Phys. Chem. C 2013, 117, 19189−19194

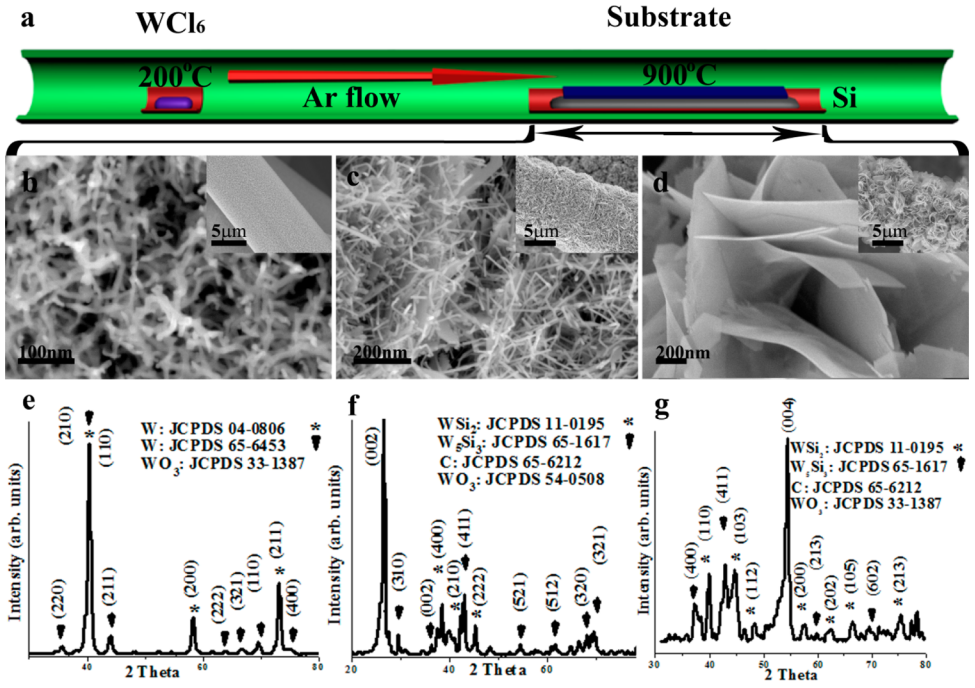

Figure 1. Growth of tungsten based nanostructure via a one-step CVD method. (a) Schematic diagram of CVD setup. SEM and XRD patterns of (b, e) W networked nanorods, (c, f) WSi_x nanonets, and (d, g) nanosheets.

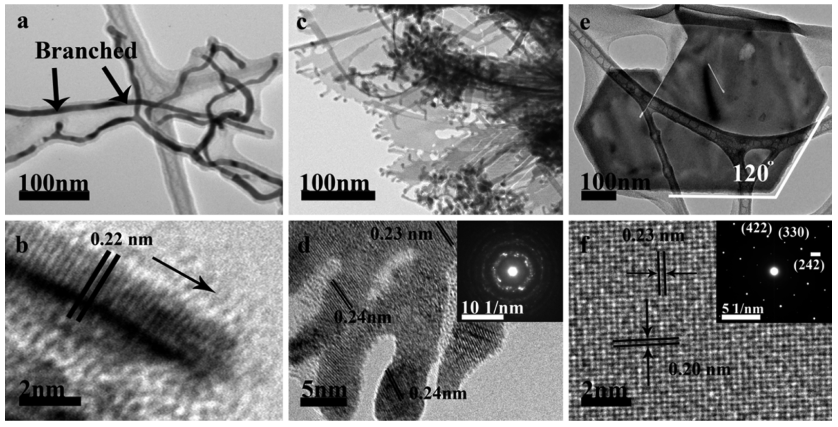

Figure 2. Morphology and structure of various nanomaterials deposited on the substrate depending on the concentration of tungsten species. (a, b) Tungsten NNWs, (c, d) tungsten disilicide NRNs, and (e, f) tungsten disilicide NS.

substrates were placed inside a quartz tube. The tube was mounted horizontally in an electric furnace. WCl_6 powders were positioned in the low-temperature region (200 °C), and Si powders were situated in the high-temperature region (900 °C). The system was purged of oxygen by decreasing the pressure to 1 mbar followed by flushing argon gas (Ar) into the system several times. The system was then heated to a set temperature with a heating rate of 10 °C·min^{-1} and kept at the temperature for 1 h. In this period the pressure was kept at 5 mbar with a continuous flow of Ar (99.99% in purity). After cooling down to room temperature a dark layer was deposited on the substrates. Figure 1a illustrates the schematic arrangement of the CVD setup for the growth of tungsten silicide nanostructures.

The morphology of the products was observed under field emission scanning electron microscope (FE-SEM, Hitachi S4800) operated at 5.0 kV equipped with energy dispersive X-ray analysis (EDX), transmission electron microscope operated at an accelerating voltage of 100 kV (TEM, Hitachi 7000). Further detailed morphology characterization was carried out by high-resolution transmission electron microscope (HRTEM, JEOL 2010) and selected area electron diffraction (SAED) operated at 200 kV. The crystal structure and composition of the products was characterized by X-ray diffractrometer using Cu Kα (λ = 0.154 nm) radiation operated at 30 kV and 15 mA (XRD, Bruker D8). Electrochemical behavior of the samples was evaluated by cyclic voltammetry in 0.5 M H_2SO_4 saturated with N_2 at room temperature using an Autolab potentiostat/galvanostat (model PGSTAT-30) scanned from −658 mV to 542 mV versus a saturated Hg/$HgSO_4$ (K_2SO_4) reference electrode at a scanning rate of 50 mV·s^{-1}.

RESULTS AND DISCUSSION

Morphological and Structural Characterization. Figure 1 summarizes the various nanostructures synthesized on the

dx.doi.org/10.1021/jp404444p | J. Phys. Chem. C 2013, 117, 19189−19194

carbon substrate in a single CVD experiment. Scanning electron micrographs (SEM, Figure 1b–d) show the three typical three-dimensional (3D) complex nanostructures changing from networked nanowires (Figure 1b, NNWs) to nanoribbon nets (Figure 1c, NRNs) and nanosheets (Figure 1d, NSs). These nanostructures were deposited at different spatial locations on the substrate. The diameter or thickness of the three morphologies, are commonly in the range of 6–10 nm. NNWs have an average diameter of 7 nm and lengths up to several micrometers. NRNs and NSs are below 10 nm in thickness, while their width and length are about few micrometers.

XRD patterns (Figure 1e–g) reveal that these nanostructures have different crystalline structures and composition. The XRD pattern of NNWs (Figure 1e) confirms the presence of two major tungsten crystal structures (JCPDS 04-0806, 65-6453). The weaker peaks can be assigned to WO_3 crystal structures. The results from NRNs and NSs (Figures 1f and g) show the presence of two types of silicides (W_5Si_3, JCPDS 65–1617; WSi_2, JCPDS 11–0195).

HRTEM characterization of the obtained nanostructures further reveals the networked nature of these nanostructures. Figure 2 shows HRTEM images of tungsten-based nanostructures and their evolution from tungsten networked nanowires (NNWs) into nanosheets (NSs). SAED patterns of these nanostructures reveal the crystalline nature of these complex nanostructures. Further observations of NNWs (Figure 2a) reveal a thin layer of 2 nm, covering the nanostructures and resulting in a core shell nanostructure. EDX analyses of these nanostructures (Supporting Information, Figure S1) indicate the presence of high atomic percentage of silicon and oxygen. This is attributed to the silicon oxide layer covering the NNWs. HRTEM image of these NNWs reveals clear lattice fringes, indicating a crystal structure with small or no defects. The *d* spacing of 0.22 nm measured from the HRTEM (Figure 2b) corresponds to (210) plane of cubic metal tungsten, confirming the tungsten cubic structure (JCPDS 65-6453) of the NNWs with [210] growth direction.

The TEM image of NRNs (Figure 2c) clearly shows ribbon and wall-like structures and the nanorods on the edges of these nanostructures forming net-like structures. The length of these nanorods is between 10 and 30 nm. The SAED pattern of these nanostructures (inset of Figure.2d) shows ring-like structures, indicating the presence of polycrystalline nanostructures. The SAED pattern reveals the presence of cubic WSi_2, partially confirmed by an XRD pattern (Figure 1f). HRTEM analyses of these nanostructures (Figure 2d) indicate an increase in the distance between lattice fringes between nanosheets (0.23 nm corresponding to $(2\bar{4}2)$ lattice planes of WSi_2 crystal structure) and nanorods (0.24 nm). This can be attributed to change in the crystal morphology of these nanostructures.

Figure 2e shows TEM image of a single NS formed on the substrate. As seen in the image, the nanosheet nanostructures form trapezoid shapes with relatively sharp edges, exhibiting 120° angles. These nanostructures usually have few imperfections as shown in Figure 2e. The SAED pattern of these nanostructures confirms that these nanostructures have a cubic WSi_2 crystal structure. The spacing between the lattice fringes also corresponds to the $(2\bar{4}2)$ and (404) lattice planes. This suggests that the nanosheets grow along equivalent planes enclosed with {111} planes of a cubic crystal structure (WSi_2).

Growth Mechanism. For catalyst-assisted growth of nanostructures, the vapor–liquid–solid growth (VLS) mechanism has been widely accepted.[1,31,32] The presence of solidified droplets at tip of synthesized nanostructures is often considered to be the evidence of a VLS mechanism. In our study, however, no catalyst was employed for the growth of tungsten based nanostructures. TEM observations did not reveal the formation of any droplets at the tips of the nanostructures, indicating that VLS is not the primary growth mechanism of the tungsten based nanostructures.

There have been several reports on the synthesis of various silicide thin films and nanostructures such as MnSi,[33] FeSi,[26] $TiSi_2$,[11] WSi_2,[34] and NiSi[12] using metal chlorides. In these studies, silicon wafers were mainly used as substrates and the silicon source. The growth mechanism proposed was based on the reduction of metal chlorides and thereby the resultant formation of silicides and $SiCl_x$. It was further believed that $SiCl_x$ could also induce the formation of silicides on Si substrates, following the vapor–solid (VS) growth route. In VS-based growth processes, partial pressures of reactive species and crystal structure of nanomaterials are key factors in determining the composition and morphology of resultant nanostructures.

Based on our experimental results, the VS growth mechanism is proposed for the growth of tungsten-based nanostructures. However, different from the previous reports as discussed above, the silicide nanostructures in this study are mainly deposited on a nonsilicon substrate. In other words, the synthesis of the tungsten silicide nanostructures in this study features the evaporation of both silicon and tungsten reactive species.

Based on the above discussion and contributions of Thomas et al.[34] from their simulation and experimental results, we speculate that our deposition of tungsten silicide on the substrate have taken the following routes:

$$2WCl_6 + 3Si \rightarrow 2W + 3SiCl_4 \quad (1)$$

$$6WCl_6 + 14Si \rightarrow W_5Si_3 + WSi_2 + 9SiCl_4 \quad (2)$$

$$SiCl_4 + 2H_2O \rightarrow SiO_2 + 4HCl \quad (3)$$

In the above reactions, the formation of silicon chloride species by the reduction of metal chlorides has also been proposed for the deposition of other silicides such as $TiSi_2$.[35] In particular, the formation of tungsten and silicon chloride vapors in reaction 1 and the formation of silicides in reaction 2 are in good agreement with our results obtained on nonsilicon based substrates.

In this study, ascribed to the nature of CVD processes and the use of powder-based source materials, the concentration of WCl_6 decreases along the chamber as it continuously reacts with Si to form tungsten-based nanostructures. Upon this point, EDX results (Supporting Information, Figure S1) and XRD results (Figure 1) provided the direct evidence. Thus, it is believed that the formation of various tungsten based nanostructures is closely related to the gradient concentration of WCl_6 along the chamber, especially along the substrate. EDX analyses (Supporting Information, Figure S1) of the three types of nanostructure show the presence of oxygen, tungsten, and silicon in all of the morphologies. It can be seen that NNWs have the highest tungsten to silicon (W/Si) ratio. The W/Si ratio decreases in NRNs and NSs. This trend is consistent with the XRD patterns (Figure 1e–g), suggesting a decrease in the density of tungsten species along the CVD chamber compared to silicon species.

dx.doi.org/10.1021/jp404444p | J. Phys. Chem. C 2013, 117, 19189–19194

NNWs Growth Mechanism. Thomas et al.[34] have reported that, under high tungsten chloride partial pressures and in the presence of lower partial pressures of silane, the formation of tungsten thin film dominates the deposition of other types of tungsten silicides. In this study, at the initial section of the reaction area (silicon powder containing section), where the concentration of WCl_6 is highly dominant compared to Si, based on reaction 1, tungsten networked nanorods are formed. At this stage, $SiCl_4$ reacts with residual oxygen in the system (oxygen trapped between powders, leakage in the system and in carrier gas) forming a thin layer of SiO_2 (reaction 3) around the tungsten network structures (Figure 2a,b).

The branching of NNWs (networked structure) is clearly marked in Figure 2a. Based on the published reports on the synthesis of branched nanostructures, branching can be induced by several processes. The branched growth is mainly reported in vapor−liquid−solid (VLS) based processes. In this growth mechanism, either catalyst nanoparticle is added to the growth process sequentially (sequential seeding) or the catalyst nanoparticles are formed during the synthesis procedure (in situ seeding).[36]

The branched and complex nanostructures can also be obtained without catalyst induced growth, such as growth by occurrence of phase transition or difference in surface energy of crystal structures.[36] In these methods, the growth process is mainly based on VS mechanism. The growth of branched nanostructures is achieved, by anisotropic growth of crystal structures from different crystal planes with different surface energies. This difference can be intrinsic of the crystal structure or can be induced by passivation of specific crystal planes. In this study, it is predicted the NNWs grow via VS growth mechanism. The networked nature of NNWs is induced by anisotropic growth crystal structures.

NRNs and NSs Growth Mechanism. In the middle and end sections of the reaction area, the concentrations of the two reactive species are balanced due to depletion of tungsten chloride and increase in the partial pressure of Si (due to presence of silicon powder), and consequently tungsten silicide compounds are formed (reaction 2). This is in accordance with simulation and experimental results reported by Thomas et al.[34]

Based on the HRTEM analysis of NRNs and NSs (Figure 2c−f), these two types of nanostructures share similar nanowall-like structures. This indicates a similar growth condition in their deposition areas.

It is interesting to note that in this section nanosheet and nanoribbon-like structures have grown on a low surface energy crystal plane. Previously, there have been many reports on the growth of nanosheets and nanoribbons. Zhang et al.[37] reported the synthesis of Al_2O_3 nanobelts. They proposed that the excessive supersaturation level of aluminum suboxide and high oxygen partial pressure in the synthesis process play key roles in the formation of 2D nanostructures. Furthermore, Ye et al.[38] have claimed that the nonequilibrium kinetic growth caused by high supersaturation of reactive species may allow the formation of a low surface energy tip, which favors 2D growth of the nanostructures.

In contrast to the above-discussed work, the nanostructures formed in our work are not synthesized in the low surface energy direction (evident from HRTEM images and SAED pattern in Figure 2f and d). Further, experimental results indicate that the increase in the partial pressure of oxygen reduces the density of 2D nanostructures and promotes the growth of WSi_2 networked nanowires.

The effect of oxygen partial pressure on the growth of silicide, sulfides, and metals nanocrystals such as FeSi[26] and digenite[39] via metal chloride precursors was studied by Zhang et al.[26,39] They reported the controlled growth of nanosheets and nanowires by controlling SiO_2 vapor pressure via oxygen partial pressure. Zhang et al[26,39] showed that SiO_2 vapor pressure plays an important role in the determining the morphology of nanostructures. They proposed a growth mechanism based on partial coverage of low surface energy planes nanocrystals by silica sheath, such as (111) planes in a digenite FCC crystal. In this mechanism, at the first stage silica clusters are adsorbed onto only several of many low surface energy planes (e.g., 2 of 8 (111) planes in FCC structure) crystal seeds due to low silica vapor pressure. At the second stage, since the silica vapor pressure is low, the silica sheath coverage will reach the critical level on some of the crystal planes rather than simultaneously on all of the similar planes. At this stage, the 2D growth of nanocrystals is induced due to the positive feedback between the imbalance of silica coverage on different planes and the net mass diffusion associated with the imbalance.[39] This process leads to faster growth of nanosheets with clear facets.

In our case, we propose that, under our experimental conditions, the partial pressure of oxygen in the system is induced by air leakage, residue oxygen, and oxygen trapped in the system. Under the low oxygen partial pressure, silica vapor is formed via silicon partial pressure over the silicon substrate and by following reaction 3. At the first stage, a layer of W_5Si_3 is formed on the substrate (supported by XRD and HRTEM results) which provides a suitable substrate for the formation of WSi_2 nuclei. In the second stage, following the growth mechanism proposed by Zhang et al.,[39] the silica clusters are formed on one of the (111) planes of the WSi_2 cubic crystal. At the third stage, the silica coverage of the (111) plane reaches a critical point, causing an imbalance of silica coverage which results in net mass diffusion of tungsten and silicon species on to (121) planes and growth of nanoribbons and nanosheets.

The growth of nanorods on the tip of nanoribbons can be attributed to decrease in the partial pressure of WCl_x near the end of the experiment. This results in the increase of silicon partial pressure and consequently the increase of silica vapor pressure. At these conditions, based on the proposed growth mechanism, the synthesis of WSi_2 nanowires and nanosheets occur simultaneously, resulting in the formation of NRNs with small nanorods at their tips (Figure 1c).

To further understand the growth mechanism of WSi_2 nanostructures, a time-dependent growth study was carried out. As seen in Figure 3, at the initial stages of the synthesis process (Figure 3a, 5 min) the substrate is covered by a thick layer composed of nanoparticles with diameters below 5 nm (formation of W_5Si_3 layer). Based on previous studies,[34] the formation of W_5Si_3 is favorable compared to WSi_2 in higher tungsten chloride and lower hydrogen partial pressures, so in the beginning of the experiments W_5Si_3 thin film is formed. At this stage, small networked nanorod and nanosheet-like structures are seen to growth on top of the deposited layer. This result confirms the growth of tungsten silicide starts from the substrate. At this stage, the nanoparticles act as nuclei for the growth of complex nanostructures.

By increasing the time (Figure 3b, 15 min), a low density of networked nanoribbons is synthesized on the deposited layer. These nanostructures, compared to NRNs shown in Figure 1c, have a similar morphology and structure. A further increase in

dx.doi.org/10.1021/jp404444p | J. Phys. Chem. C 2013, 117, 19189−19194

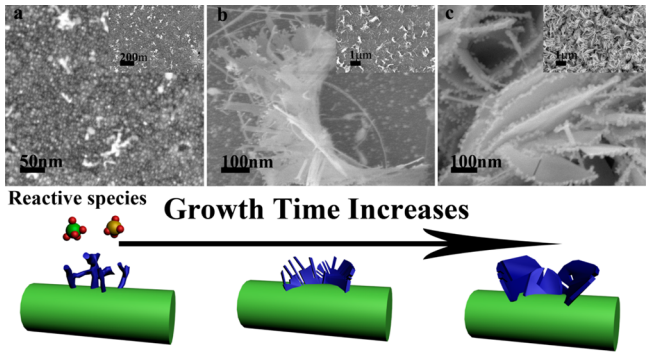

Figure 3. Time-dependent evolution of nanoparticles into NSs: (a) 5 min, (b) 15 min, and (c) 45 min. (d) Schematic diagram of growth processes of NSs.

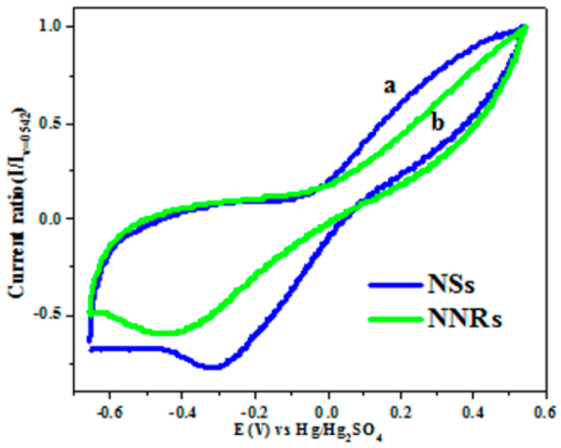

Figure 4. Normalized cyclic voltammetry of the WSi_2 nanostructures (a) NSs and (b) NNRs.

time (Figure 3c, 45 min) resulted in the high density growth of NSs. Figure 3d shows a schematic illustration of growth of WSi_2 nanostructures.

These results illustrate the evolution of NRNs into NSs, suggesting the dependence of WSi_2 NSs growth on the partial pressure of reactive species (specifically WCl_6 and oxygen) and growth time. The increase in time increases the amount of reactive species reaching the growth front of the nanostructures (similar to higher concentration at a shorter time). At this point, the nanostructures start to grow in two dimensions filling the voids between the nanoribbons and forming nanosheets.

To validate the above growth mechanism and demonstrate the control over the nanostructures deposited on the substrate, additional experiments were carried out with controlling the oxygen content in the CVD chamber. The oxygen content is directly related to the silica partial pressure in the CVD chamber. By increasing the oxygen content in the CVD chamber via introduction of oxygen along with Ar as carrier gas, a uniform layer of tungsten nanowires were deposited along the CVD chamber with a very small area of tungsten silicide nanostructures. Figure S2a and b (Supporting Information) shows SEM images of tungsten nanowires synthesized on the substrate under O_2 (5%) + Ar carrier gas flow. Figure S2c and d shows SEM images of tungsten silicide nanostructures synthesized under H_2 (2%) + Ar. Thick nanosheets are synthesized on the substrate. The higher thickness is believed to be due to lack of oxygen. This delays the formation of SiO_2 on the nanostructures, leading to thicker nanostructures.

Recent reports have shown that nanostructures with various morphologies exhibit different capacitance performances.[40,41] Therefore we have studied the electrochemical capacitance behavior of WSi_2 nanostructures synthesized using the CVD method. Figure 4 shows the normalized cyclic voltammograms of the WSi_2 nanostructures without any pretreatment. From comparisons of the area under curves a and b in Figure 4, it is apparent that WSi_2 NSs have a larger area than the WSi_2 NNRs. This indicates that the WSi_2 nanosheets have a higher capacitance than that of WSi_2 networked nanoribbons. Similar to previous reports, this can be due to the higher surface and larger micropore area of the nanosheets compared with the networked nanoribbons.[40,41] This result implies that WSi_2 nanostructures especially nanosheet morphologies could be considered as promising material in the application of nanodevices for electrochemical energy storage. However, due to the presence of SiO_2 shell layer, it is a challenge to calculate the exact capacity of the nanostructures. Further study is needed in our work.

CONCLUSIONS

For the first time, we have synthesized single crystalline WSi_2 nanonets and nanosheets on carbon paper substrates using a one-step LPCVD method. The concentration changes of the tungsten precursor and partial pressure of oxygen can results in the formation of products with a wide range of morphologies and composition. The growth mechanism of the tungsten silicide nanostructures is proposed based on the formation of silica sheath on several (111) on nuclei of WSi_2 nanostructures and morphological evolution with the growth time. These nanostructures are formed in three stages: (i) forming nanoparticles, (ii) growing into nanonets, and (iii) evolving to nanosheets. Cyclic voltammetry measurements of the nanostructures indicate that WSi_2 nanostructures show superior electrochemical capacitance with WSi_2 NSs exhibiting higher capacitance compared to WSi_2 NNRs. These nanostructures could be potential material for nanodevices and electrochemical applications.

ASSOCIATED CONTENT

Supporting Information

EDX spectrum and the atomic ratio of elements in the various nanostructures (Figure S1). The results indicate the general increase in the atomic ratio of oxygen content in the nanostructures and decrease of tungsten and silicon atomic ratio. This has been correlated to the depletion of WCl_x reactive species, and release of oxygen trapped between the silicon source powders along the CVD chamber, resulting in the formation of various nanostructures. SEM images of nanostructures synthesized under various composition of carrier gas flow are shown in Figure S2. This material is available free of charge via the Internet at http://pubs.acs.org.

AUTHOR INFORMATION

Corresponding Author

*E-mail: xsun@eng.uwo.ca. Tel.: +1 (519) 661-2111 ext. 87759. Fax: +1 (519) 661-3020.

Notes

The authors declare no competing financial interest.

■ ACKNOWLEDGMENTS

This research was supported by General Motors of Canada, Ontario Centres of Excellence, Natural Sciences and Engineering Research Council of Canada, Canada Research Chair Program, Canada Foundation for Innovation, and the University of Western Ontario.

■ REFERENCES

(1) Zhang, Y.; Geng, D.; Liu, H.; Banis, M. N.; Ionescu, M. I.; Li, R.; Cai, M.; Sun, X. Designed Growth and Characterization of Radially Aligned Ti_5Si_3 Nanowire Architectures. *J. Phys. Chem. C* **2011**, *115*, 15885−15889.

(2) Wen, C. Z.; Hu, Q. H.; Guo, Y. N.; Gong, X. Q.; Qiao, S. Z.; Yang, H. G. From Titanium Oxydifluoride ($TiOF_2$) to Titania (TiO_2): Phase Transition and Non-metal Doping with Enhanced Photocatalytic Hydrogen (H2) Evolution Properties. *Chem. Commun.* **2011**, *47*, 6138−6140.

(3) Zhou, S. Spontaneous Growth of Highly Conductive Two-Dimensional Single-Crystalline $TiSi_2$ Nanonets. *Angew. Chem., Int. Ed.* **2008**, *47*, 7681−7684.

(4) Chou, L.-J.; Chueh, Y.-L.; Ko, M.-T. Interconnect and Contact for Nanoelectronics: Metallic $TaSi_2$ Nanowires. *Thin Solid Films* **2007**, *515*, 8109−8112.

(5) Kim, T.; Bird, J. P. Electrical Signatures of Ferromagnetism in Epitaxial $FeSi_2$ Nanowires. *Appl. Phys. Lett.* **2010**, *97*, 263111−263114.

(6) Schmitt, A. L.; Higgins, J. M.; Szczech, J. R.; Jin, S. Synthesis and Applications of Metal Silicide Nanowires. *J. Mater. Chem.* **2010**, *20*, 223−235.

(7) Jiang, S.; Xin, Q.; Chen, Y.; Lou, H.; Lv, Y.; Zeng, W. Preparation of NiSi2 Nanowires with Low Resistivity by Reaction Between Ni Coating and Silicon Nanowires. *Appl. Phys. Exp.* **2009**, *2*, 075005.

(8) Zou, C.; Zhang, X.; Jing, G.; Zhang, J.; Liao, Z.; Yu, D. Synthesis and Electrical Properties of $TiSi_2$ Nanocables. *Appl. Phys. Lett.* **2008**, *92*, 253102−253105.

(9) Lin, Y.; Zhou, S.; Liu, X.; Sheehan, S.; Wang, D. $TiO_2/TiSi_2$ Heterostructures for High-Efficiency Photoelectrochemical H_2O Splitting. *J. Am. Chem. Soc.* **2009**, *131*, 2772−2773.

(10) Zhou, S.; Liu, X.; Wang, D. $Si/TiSi_2$ Heteronanostructures as High-Capacity Anode Material for Li Ion Batteries. *Nano Lett.* **2010**, *10*, 860−863.

(11) Zhou, S.; Liu, X.; Lin, Y.; Wang, D. Rational Synthesis and Structural Characterizations of Complex $TiSi_2$ Nanostructures. *Chem. Mater.* **2009**, *21*, 1023−1027.

(12) Zhang, H.-L.; Li, F.; Cheng, H.-M. The Facile Synthesis of Nickel Silicide Nanobelts and Nanosheets and Their Application in Electrochemical Energy Storage. *Nanotechnology* **2008**, *19*, 1−7.

(13) Cheb, J. L. Metal Silicides: An Integral Part of Microelectronics. *J. Org. Mater.* **2005**, *57*, 24−30.

(14) Chirkin, A. D.; Lavrenko, V. O.; Talash, V. M. High-Temperature and Electrochemical Oxidation of Transition Metal Silicides. *Powder Met. Met. Ceram.* **2009**, *48*, 330−345.

(15) Mitra, R. Mechanical Behaviour and Oxidation Resistance of Structural Silicides. *Int. Mater. Rev.* **2006**, *51*, 13−64.

(16) Meschter, P. J.; Schwartz, D. S. Silicide-Matrix Materials for High-Temperature Applications. *J. Org. Mater.* **1989**, *41*, 52−55.

(17) Liu, H. J.; Owen, J. H. G.; Miki, K.; Renner, C. Manganese Silicide Nanowires on Si(001). *J. Phys.: Condens. Matter* **2011**, *23*, 172001−172006.

(18) Wen, Z.; Ji, S.; Sun, J.; Tian, F.; Tian, R.; Xie, J. Mechanism of Lithium Insertion into $NiSi_2$ Anode Material for Lithium Ion Batteries. *Rare Met.* **2006**, *25*, 77−81.

(19) Fitzer, E.; Remmele, W. Silicide and Modified Silicide Coatings for High Temperature Applications. *Mater. Sci. Eng.* **1987**, *88*, 349.

(20) Patnaik, P. C. Intermetallic Coatings for High Temperature Applications - a Review. *Mater. Manuf. Process* **1989**, *4*, 133−152.

(21) Szczech, J. R.; Jin, S. Epitaxially-Hyperbranched FeSi Nanowires Exhibiting Merohedral Twinning. *J. Mater. Chem.* **2010**, *20*, 1375−1382.

(22) Szczech, J. R.; Schmitt, A. L.; Bierman, M. J.; Jin, S. Single-Crystal Semiconducting Chromium Disilicide Nanowires Synthesized via Chemical Vapor Transport. *Chem. Mater.* **2007**, *19*, 3238−3243.

(23) Varadwaj, K. S. K.; Seo, K.; In, J.; Mohanty, P.; Park, J.; Kim, B. Phase-Controlled Growth of Metastable Fe_5Si_3 Nanowires by a Vapor Transport Method. *J. Am. Chem. Soc.* **2007**, *129*, 8594−8599.

(24) Higgins, J. M.; Ding, R.; Jin, S. Synthesis and Characterization of Manganese-Rich Silicide (α-Mn_5Si_3, β-Mn_5Si_3, and β-Mn_3Si) Nanowires. *Chem. Mater.* **2011**, *23*, 3848−3853.

(25) Chueh, Y.-L.; Ko, M.-T.; Chou, L.-J.; Chen, L.-J.; Wu, C.-S.; Chen, C.-D. $TaSi_2$ Nanowires: a Potential Field Emitter and Interconnect. *Nano Lett.* **2006**, *6*, 1637−1644.

(26) Zhang, H.-X.; Ge, J.-P.; Wang, J.; Li, Y.-D. Atmospheric Pressure Chemical Vapour Deposition Synthesis of Sulfides, Oxides, Silicides and Metal Nanowires with Metal Chloride Precursors. *Nanotechnology* **2006**, *17*, 253−261.

(27) Lin, Y.; Zhou, S.; Sheehan, S. W.; Wang, D. Nanonet-Based Hematite Heteronanostructures for Efficient Solar Water Splitting. *J. Am. Chem. Soc.* **2011**, *133*, 2398−2401.

(28) Elmalem, E.; Saunders, A. E.; Costi, R.; Salant, A.; Banin, U. Growth of Photocatalytic CdSe−Pt Nanorods and Nanonets. *Adv. Mater.* **2008**, *20*, 4312−4317.

(29) Schultes, G.; Schmitt, M.; Goettel, D.; Freitag-Weber, O. Strain Sensitivity of TiB_2, $TiSi_2$, $TaSi_2$ and WSi_2 Thin Films as Possible Candidates for High Temperature Strain Gauges. *Sens. Actuators Phys.* **2006**, *126*, 287−291.

(30) Reader, A. H.; van Ommen, A. H.; Weijs, P. J. W.; Wolters, R. A. M.; Oostra, D. J. Transition Metal Silicides in Silicon Technology. *Rep. Prog. Phys.* **1993**, *56*, 1397−1467.

(31) Banis, M. N.; Zhang, Y.; Banis, H. N.; Li, R.; Sun, X.; Jiang, X.; Nikanpour, D. Controlled Synthesis and Characterization of Single Crystalline MnO Nanowires and Mn−Si Oxide Heterostructures by Vapor Phase Deposition. *Chem. Phys. Lett.* **2011**, *501*, 470−474.

(32) Rao, C. N.; Deepak, F.; Gundiah, G.; Govindaraj, A. Inorganic Nanowires. *Prog. Solid State Chem.* **2003**, *31*, 5−147.

(33) Higgins, J. M.; Ding, R.; Degrave, J. P.; Jin, S. Signature of Helimagnetic Ordering in Single-crystal MnSi Nanowires. *Nano Lett.* **2010**, *10*, 1605−1610.

(34) Thomas, N.; Dutron, A. M.; Vahlas, C.; Bernard, C.; Madar, R. Influence of Hydrogen Pressure on the Properties of CVD Tungsten Silicide Films. *J. Electrochem. Soc.* **1995**, *142*, 1608−1614.

(35) Bouteville, A.; Remy, J. C.; Attuyt, C. $TiSi_2$ Selective Growth in a Rapid Thermal Low Pressure Chemical Vapor Deposition System. *J. Electrochem. Soc.* **1992**, *139*, 2260−2263.

(36) Liu, X.; Lin, Y.; Zhou, S.; Sheehan, S.; Wang, D. Complex Nanostructures: Synthesis and Energetic Applications. *Energies* **2010**, *3*, 285−300.

(37) Zhang, Y.; Li, R.; Zhou, X.; Cai, M.; Sun, X. Selective Growth of α-AI_2O_3 Nanowires and Nanobelts. *J. Nanomater.* **2008**, 1−8.

(38) Ye, C.; Fang, X.; Hao, Y.; Teng, X.; Zhang, L. Zinc Oxide Nanostructures: Morphology Derivation and Evolution. *J. Phys. Chem. B* **2005**, *109*, 19758−19765.

(39) Zhang, H.-X.; Ge, J.-P.; Li, Y.-D. Geometrically Kinetic Competition Mechanism to Shape Control on Digenite Nanocrystals with Silica Vapor in APCVD. *J. Phys. Chem. B* **2006**, *110*, 14107−14113.

(40) Xiong, S.; Yuan, C.; Zhang, X.; Xi, B.; Qian, Y. Controllable Synthesis of Mesoporous Co_3O_4 Nanostructures with Tunable Morphology for Application in Supercapacitors. *Chem.−Eur. J.* **2009**, *15*, 5320−5326.

(41) Yang, S.-Y.; Chang, K.-H.; Tien, H.-W.; Lee, Y.-F.; Li, S.-M.; Wang, Y.-S.; Wang, J.-Y.; Ma, C.-C. M.; Hu, C.-C. Design and Tailoring of a Hierarchical Graphene-carbon Nanotube Architecture for Supercapacitors. *J. Mater. Chem.* **2011**, *21*, 2374−2380.